How Does the Synergism Work?

A stable and non-precious double-atom catalyst was demonstrated for the next generation of superior oxygen-evolution catalysts.

The oxygen-evolution reaction (OER) is an important electrochemical anodic reaction that provides protons and electrons for fuel-generating cathodic reactions such as the hydrogen-evolution reaction and CO_2 reduction reactions. Tremendous efforts have been made to develop efficient and scalable OER electrocatalysts. For instance, mixed metal oxides containing Co, Fe or Ni have been found to be the most active heterogeneous OER catalysts in an alkaline medium, but the heterogeneous nature of these metal oxides makes it difficult to study and to understand the fundamental properties and mechanisms of these catalysts. Fortunately, atomically dispersed catalysts including single-atom catalysts and discrete sub-nano clusters are an emerging class of heterogeneous electrocatalysts with high atomic efficiency. These catalysts possess uniform and well defined active sites, providing a unique opportunity for a mechanistic understanding.

Xile Hu (Ecole Polytechnique Fédérale de Lausanne, Switzerland) and Hao Ming Chen (National Taiwan University) recently developed a general synthesis of Co-, Fe- and Ni-containing double-atom catalysts from their single-atom precursors *via* electrochemical transformation *in situ*. Employing *operando* X-ray absorption spectra (XAS) at beamlines **TPS 44A**, **TLS 01C1**, **SP 12B1** and **SP 12U1**,[1] the results demonstrated how atomic-configuration and chemical state could affect their resulting catalytic nature. For example, *operando* extended X-ray absorption fine structure (EXAFS) spectra of the Ni K-edge and the Fe K-edge were recorded under varied conditions, as plotted in **Fig. 1**. The results indicated that the Ni ion in Ni–N–C is most probably coordinated with 3N, 1C and 1O. The N and C donors come from the N-doped carbon support; the O donor is assumed to be an adsorbed hydroxyl group or water. When a single-atom Ni catalyst (Ni–N–C) was immersed in 1-M KOH, two N donors were replaced by three new O donors (OH^-/H_2O), as shown in **Fig. 1(a)**. After five cyclic voltammetry scans

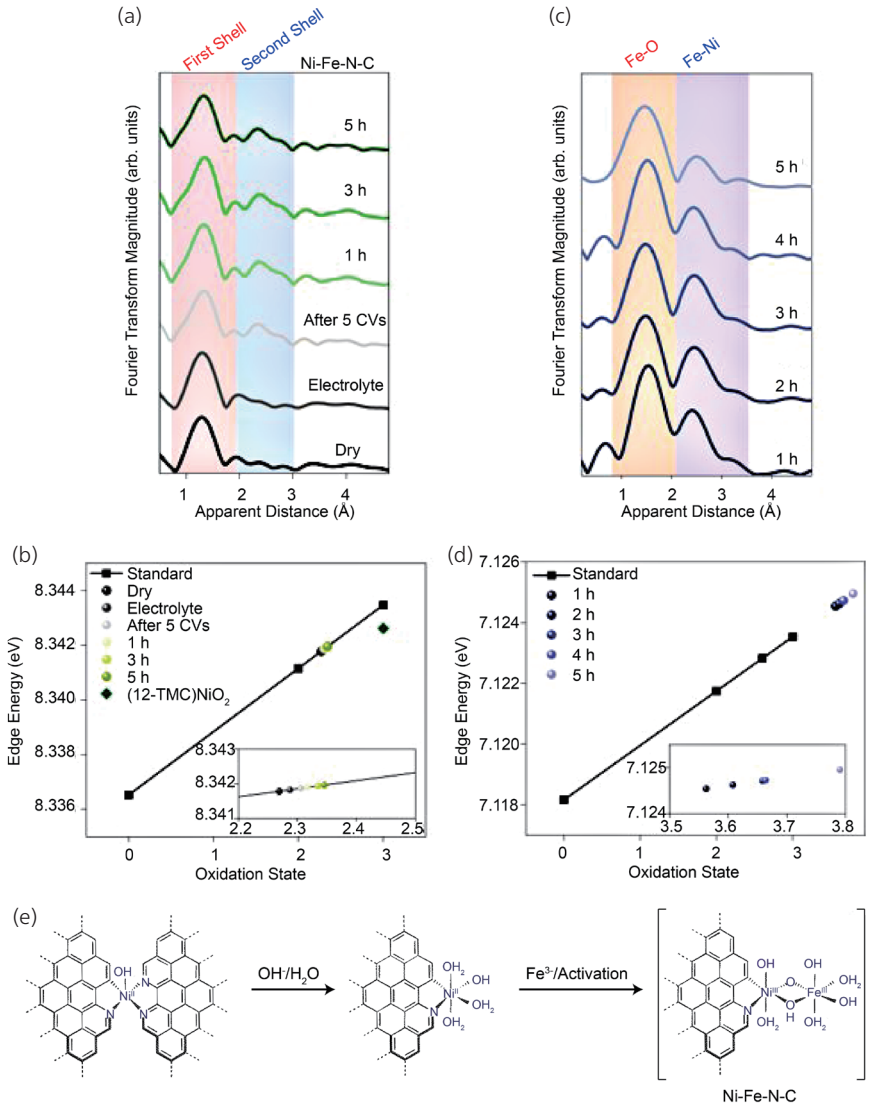

Fig. 1: *Operando* XAS study of Ni–Fe–N–C. (a) *Operando* EXAFS spectra of Ni K-edge for Ni–N–C (as prepared) and Ni–Fe–N–C under various conditions. (b) Edge-jump energies of Ni K-edge spectra for Ni–N–C (as prepared) and Ni–Fe–N–C under various conditions. Inset: enlarged graph for the oxidation states. (c) *Operando* EXAFS spectra of Fe K-edge for Ni–Fe–N–C under various reaction durations. (d) Edge-jump energies of Fe K-edge spectra for Ni–Fe–N–C under various reaction durations. Inset: enlarged graph for the oxidation state. (e) A scheme showing the formation of double-atom Ni–Fe–N–C from the single-atom Ni–N–C precatalyst. [Reproduced from Ref. 1]

and under extended electrolysis, the first coordination shell of Ni remained nearly the same, while the second scattering shell of Fe appeared. The coordination structure of the Ni–Fe double-atom catalyst (Ni–Fe–N–C) remained stable under OER conditions on a time scale of 5 h (**Fig. 1(a)**). As displayed in **Fig. 1(b)**, the oxidation state of Ni in the dry sample was between +2 and +3. The energy of the absorption edge of Ni increased only slightly on formation of Ni–Fe–N–C and remained nearly the same during extended electrolysis, indicating that only a few Ni^{2+} ions in Ni–N–C were oxidized to Ni^{3+} on activation. As shown in **Fig. 1(d)**, after electrolysis for 1 hour, the average oxidation state of the Fe ion was greater than +3, indicating the formation of substantial Fe(IV) species during OER. The distal iron ion was initially surrounded by close to six oxygen ligands in the first shell and exhibited a Fe–Ni path in the second shell (**Fig. 1(c)**). With increasing duration of electrolysis, the gradual increase of the coordination number (CN) of Ni–Fe was related to the formation of more Ni–Fe atom pairs. The process of formation of Ni–Fe double atoms from Ni–N–C is summarized in **Fig. 1(e)**.

Compared with conventional XAS, a coordinated environment-sensitive approach of *operando* K_β high-energy-resolution fluorescence detected (HERFD)–XAS, as plotted in **Fig. 2**, was performed to investigate the characters of frontier orbitals as well as the bonding state of reactive metals. After five cyclic voltammetry cycles, the symmetry of Ni transformed to highly symmetrical octahedral because of the desorption of nitrogen and attachment of oxygen, in which the signal area of the pre-edge decreased further. This result indicates the restoration of a high symmetry at the Ni centre, which is consistent with the formation of the Ni–Fe–N–C catalyst with octahedral symmetry (**Fig. 1(e)**). During further electrolysis, the dipole transition remained largely steady (**Figs. 2(a) and 2(b)**). In the higher-energy region of the HERFD–XAS Ni K-edge spectra, a metal-to-ligand electronic transition (MLET) was observed. On immersion into the electrolyte, the intensity of the MLET substantially declined. This result is consistent with the coordination of some O ligands and the departure of one or more N ligands, as metal–O interaction is weaker than metal–N interaction. On activation with cyclic voltammetry and continuous electrolysis, the intensity of the MLET further decreased until a steady state was reached in 4 hours, indicating that iron ions continued to attach to the Ni site during initial electrolysis until an equilibrium was reached in 4 hours. As plotted in **Fig. 2(e)**, the energy split of Ni–Fe–N–C was about 1.3 eV, similar to that of $Fe(NO_3)_3$, which has six coordinated H_2O ligands of symmetry O_h. This result is attributed to a ligand field caused by H_2O ligands weaker

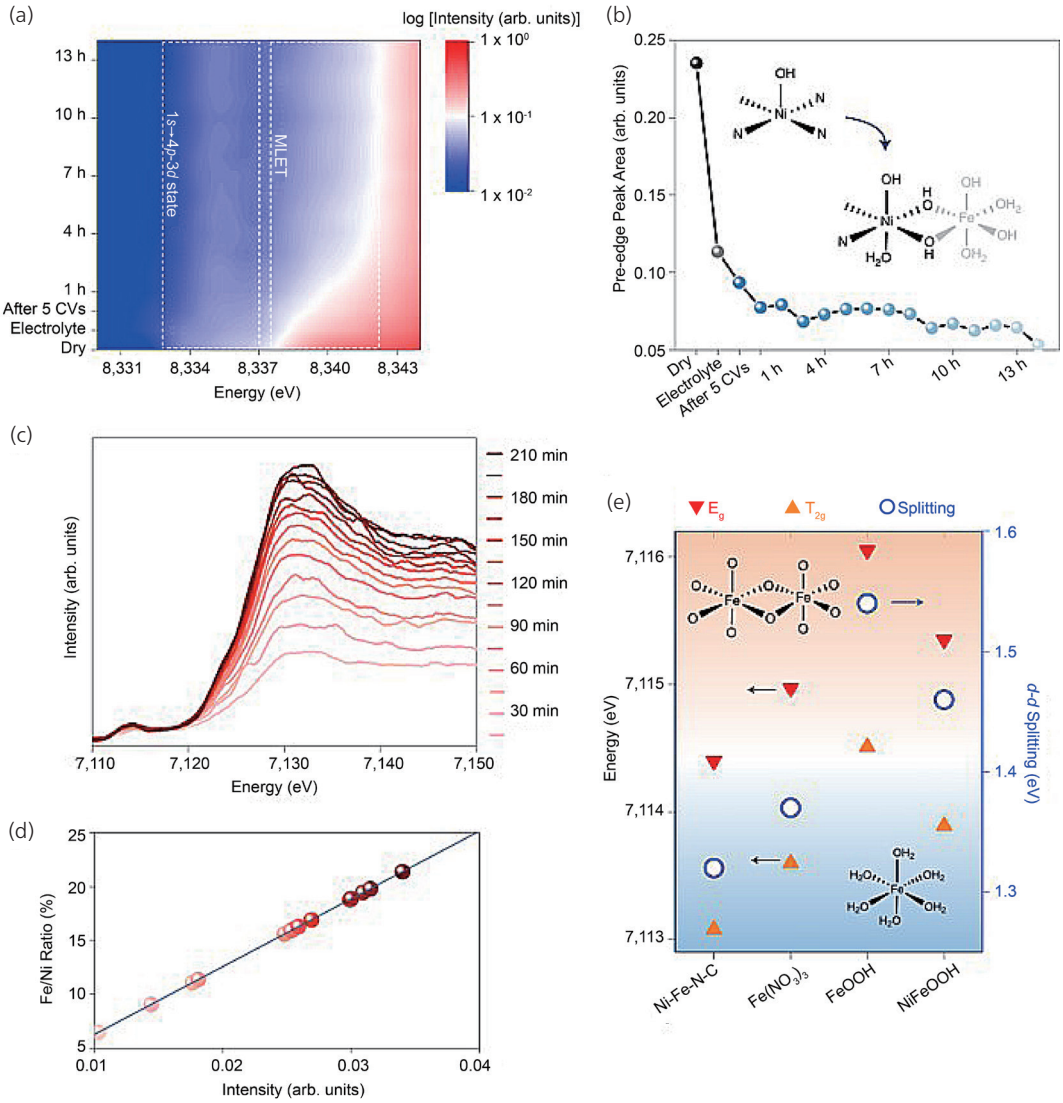

Fig. 2: *Operando* HERFD–XAS experiments of Ni–Fe–N–C. (a) *Operando* Ni K-edge HERFD–XAS of Ni–Fe–N–C, the graph is derived from the intensity of pre-edge spectra under varied conditions. (b) Integrated area of pre-edge region from 8,332 eV to 8,337 eV of Ni K-edge HERFD–XAS for Ni–Fe–N–C under varied conditions. (c) *Operando* Fe K-edge HERFD–XAS of Ni–Fe–N–C at varied durations of activation. (d) Fe:Ni ratio in Ni–Fe–N–C determined with HERFD–XAS. (e) Energy levels E_g and T_{2g}, and the ligand-field-splitting energy in Ni–Fe–N–C, $Fe(NO_3)_3$, FeOOH and NiFeOOH. [Reproduced from Ref. 1]

than for lattice oxygen atoms in FeOOH and NiFeOOH. The energy split in Ni–Fe–N–C is even smaller than that of $Fe(NO_3)_3$, probably due to a more asymmetric structure of the Ni–Fe units compared to $Fe(NO_3)_3$. All these results further support the formation of Ni–Fe double atoms.

In summary, the molecular nature of active sites in these double-atom catalysts facilitates the deduction of reaction mechanisms using data from XAS and electrokinetic measurements. In the future, the new molecular platform proposed by this team of researchers could be used to study heterogenous OER electrocatalysts in depth. For instance, it could help material scientists to understand better how an atomic configuration and chemical state of a catalyst affect its catalytic nature. (Reported by Yan-Gu Lin)

*This report features the work of Xile Hu and Hao Ming Chen published in Nat. Energy **6**, 1054 (2021).*

TPS 44A Quick-scanning X-ray Absorption Spectroscopy
TLS 01C1 EXAFS
SP 12B1 Materials X-ray Study
SP 12U1 Inelastic X-ray Scattering

- XANES, EXAFS
- Materials Science, Chemistry, Condensed-matter Physics, Environmental and Earth Science

Reference

1. L. Bai, C.-S. Hsu, D. T. L. Alexander, H. M. Chen, X. Hu, Nat. Energy **6**, 1054 (2021).

Lighting the Path to Perovskite Photovoltaics

The time-resolved grazing-incidence wide-angle X-ray scattering technique is demonstrated to study the phase transition during the formation of perovskite quantum wells.

Perovskite quantum wells (PQW) exhibit greatly enhanced stability in contrast to the traditional 3D perovskite due to the long-organic-chain ligands. In contrast to cations of smaller size, the ligand molecules with a longer chain can form an interdigitating structure at an interface stabilized by the van der Waals force, resulting in an overall stabilization of the stacked perovskite hierarchy. The photovoltaic performance of pure 2D perovskite solar cells is, however, not at par with that of its 3D counterpart because of anisotropic charge-carrier transport. To combine the excellent efficiency of light to electricity of the 3D perovskite with the desired stability of the PQW, the hierarchy of building a low-dimensional perovskite layer on top of a 3D bulk perovskite layer has been introduced. Thus far, most studies on PQW/3D perovskite have focused on the photovoltaic performance (including stability) after the formation of the hierarchy; whereas the critical issue of determining how the coated ligand molecules convert the 3D perovskite lattice into the reduced-dimensional perovskite structure is rarely explored.

Gang Li (Hong Kong Polytechnic University, China) and his coworkers recently explored in detail the formation mechanism of PQW on top of a 3D perovskite bulk layer through the real-time tracking of crystal phase evolution. Employing grazing-incidence wide-angle scattering measurements (GIWAXS) *in situ* at beamline **TLS 23A1**,[1] the results revealed the formation *in situ* of PQW when hexyltrimethylammonium bromide (HTAB) was coated on top of the 3D perovskite layer. The time-resolved GIWAXS intensity map during the spin coating of HTAB on top of the pristine 3D perovskite layer is shown in **Fig. 1(a)** (see next page). Before the HTAB dripping, only the scattering rings from the 3D perovskite crystals at a large q regime appear, as shown in **Fig. 1(b)**. After the HTAB was coated on the 3D perovskite layer, a new ordered intermediate phase immediately emerged in the low q regime (q = 0.31 Å^{-1}), as indicated by the red arrow in **Fig. 1(c)**. Surprisingly, a strikingly strong ionic reaction between the 3D perovskite and the long-chain organic cation led to the rapid formation of an ordered intermediate phase within only a few seconds, as shown in **Fig. 1(d)**. The existence of this reaction sufficiently explained the decrease in the 3D perovskite (110) scattering signal when the 2D perovskite scattering signals in the small-q regime intensified as the HTAB concentration increased. The optimal PQW/3D architecture was achieved on controlling the HTAB casting, which was assisted by time-of-flight secondary-ion mass spectral characterization. On controlling the second ionic reaction during the long-chain cation coating, along with the fluorinated poly(triarylamine) as a hole-transport layer, the perovskite solar cells demonstrated efficiencies exceeding 22% along with greatly improved device stability.

In summary, to realize efficient and stable perovskite solar cells, the profound mechanism of PQW formation in the PQWs/3D heterostructure was explored. Time-resolved GIWAXS revealed a rapid ionic reaction immediately after HTAB casting, yielding